

Cite this: DOI: 10.1039/c0xx00000x

www.rsc.org/xxxxxx

ARTICLE TYPE

Smectic mesophases of functionalized silver and gold nanoparticles with anisotropic plasmonic properties

Wiktor Lewandowski,^{*a} Doru Constantin,^b Kinga Walicka,^a Damian Pocięcha,^a Józef Mieczkowski^a and Ewa Górecka^a

5

SUPPORTING INFORMATION

1.	Materials and methods.....	S1
2.	Mesogenic ligand synthesis (L).....	S2
10 3.	Mesogenic ligand (L) phase sequence.....	S4
4.	Gold nanoparticles synthesis (G ₈).....	S4
5.	Silver nanoparticles synthesis (A ₆).....	S5
6.	Hybrid nanoparticles synthesis.....	S5
7.	XPS analysis of A ₆	S5
15 8.	¹ H NMR analysis of A ₆ L and G ₈ L.....	S6
9.	TGA analysis of A ₆ , G ₈ , A ₆ L and G ₈ L.....	S7
10.	SAXS and SAXRD analysis of A ₆ , G ₈ , A ₆ L and G ₈ L.....	S9
11.	TEM analysis of gold nanoparticles.....	S11
12.	Polarized Optical Microscopy analysis of A ₆ L.....	S11
20 13.	Polarized IR studies.....	S11
14.	UV-Vis measurements of A ₆ and A ₆ L nanoparticles solutions.....	S12
15.	Surface plasmon resonance shift calculations.....	S12

1. Materials and methods

Solvents and substrates were obtained from Sigma-Aldrich. Before use solvents were dried over activated 3 Å molecular sieves for 24h. Substrates were used without further purification. All reactions were carried out under nitrogen (N₂) atmosphere in dried glassware and assuring efficient magnetic stirring. Purification of reaction products was carried out by column chromatography using RushanTaiyang silica gel 60 (230-400 mesh) at atmospheric pressure or by crystallization if possible. Analytical thin-layer chromatography (TLC) was performed using Silica Gel 60 Å F254 (Merck) pre-coated glass plater (0.25 mm thickness) and visualized using iodine vapor and/or UV lamp (254 nm). Yields refer to chromatographically and spectroscopically (¹H NMR) homogeneous materials.

The ¹H NMR spectra were recorded at either 200 MHz or 500 MHz NMR Varian Unity Plus. The ¹³C NMR spectra were recorded at NMR Varian Unity Plus 200 MHz. Proton chemical shifts are reported in ppm (δ) relative to the internal standard – tetramethylsilane (TMS δ=0.00 ppm). Carbon chemical shifts are reported in ppm (δ) relative to the residual solvent signal (CDCl₃, δ=77.0 ppm). Data are presented as follows: chemical shift, integration, multiplicity (s = singlet, d = doublet, t = triplet, q = quartet, br = broad, m = multiplet), and coupling constant (Hz). In all recorded spectra there are also sharp signals coming from small amount of known impurities present in used solvent: H₂O (1.7 ppm) and CHCl₃ (7.27 ppm).

Differential scanning calorimetry was performed with a TA Q200 (TA Instruments). The measurement was carried out in nitrogen atmosphere with 5 K/min heating/cooling rate.

The small angle X-ray diffraction (SAXRD) patterns for the powder as well as partially aligned samples were obtained with the BrukerNanostar system. The CuKα radiation was used, patterns were registered with an area detector VANTEC2000. The temperature of the sample was controlled with precision of 0.1 K. Kapton tape was used as a substrate for nanoparticle measurements. The nanoparticle samples were first heated up to 150 °C, quickly aligned by shearing and cooled to room temperature. The same BrukerNanostar system

was also used for the scattering experiments (SAXS). The scattering data from nanoparticle solution in toluene were analyzed using NANOFIT software, assuming spherical form factor for non-interacting particles (structure factor $S=1$) and Shultz distribution of the particle sizes.

Oriented A_6L samples deposited on glass microscope coverslips were observed between crossed polarizers using an Olympus BX-51 microscope (10x objective), images were acquired using an Olympus XZ-1 camera.

X-ray photoelectron spectroscopy (XPS) experiments were performed in a PHI 5000 VersaProbe—Scanning ESCA microprobe (ULVAC-PHI, Japan/USA) instrument at a base pressure below 5×10^{-9} mbar. Monochromatic Al $K\alpha$ radiation was used and the X-ray beam, focused to a diameter of 100 μm , was scanned on a $250 \times 250 \mu\text{m}$ surface, at an operating power of 25 W. Photoelectron survey spectra were acquired using a hemispherical analyzer at pass energy 117.4 eV with a 0.4 eV energy step, core-level spectra were acquired at pass energy 23.5 eV with a 0.1 eV energy step. All spectra were acquired with 90° between X-ray source and analyzer and with the use of low energy electrons and low energy argon ions for charge neutralization. After subtraction of the Shirley-type background, the core-level spectra were decomposed into their components with mixed Gaussian–Lorentzian (30:70) shape lines using the CasaXPS software. Quantification calculations were conducted with using sensitivity factors supplied by PHI. Spectra were calibrated against 284.6 eV for C 1s region.

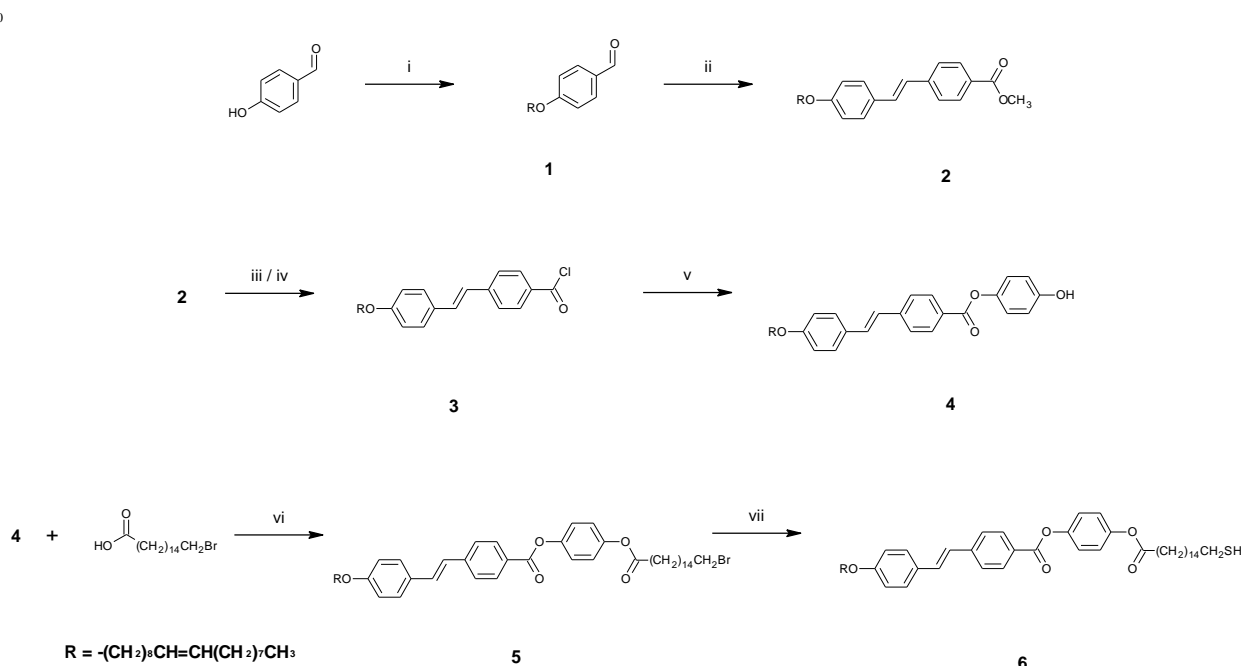
Transmission electron microscopy was performed using Zeiss Libra 120 microscope, with LaB6 cathode, equipped with OMEGA internal columnar filters and CCD camera.

Thermogravimetric analysis were performed with a TA Q50 V20.13 (TA Instruments) analyzer. The measurements were carried out in 20–600 $^\circ\text{C}$ range with 10 K/min heating rate in air.

The UV-Vis spectrum was measured using a Cary 5000 spectrometer (Agilent). The solutions of functionalized particles in cyclohexane or dichloromethane were held in standard PMMA cuvettes (VWR) with a 10 mm optical path, while the doped mesophases were deposited onto standard microscope cover slips (0.17 mm thick). In the latter case the beam was defined by a diaphragm (5 mm in diameter) placed immediately before the sample and the samples were also studied using light linearly polarized by a rotating analyzer (AN 360P, Olympus) inserted in the optical path ahead of the sample, for three orientations of the electric field (vertical, horizontal and at 45°).

IR spectra were recorded on a Nicolet 6700FT-IR spectrometer. The sample was placed on ZnSe plate, aligned by shearing and heated with a Linkam hot stage. The IR polarizer was rotated with respect to the rubbing direction in the sample to obtain variation of IR signal intensities. TEM images were taken using Zeiss Libra 120 microscope.

1. Mesogenic ligand synthesis (L)



6 - compound L in the main text

Scheme S1. Synthetic route for the preparation of mesogenic ligands: i) oleyl alcohol, DIAD, PPh_3 , THF; ii) methyl 4-(triphenylphosphoniummethyl)benzoate bromide, CH_2Cl_2 , THF, 18-crown-6; iii) KOH/EtOH , rfx; iv) $(\text{COCl})_2/\text{toluene}$; v) resorcinol, TEA, THF, DMAP, room temp., 4–5 h; vi) DCC, THF, DMAP; vii) HMDT, TBAF, THF, -10°C

Synthesis of 4-(octadec-9-enyloxy)benzaldehyde (**1**)

Triphenylphosphine (35.37 g, 0.14 mol) and oleyl alcohol (41.70 ml, 0.18 mol) was added to 4-hydroxybenzaldehyde (15.06 g, 0.12 mol) dissolved in dry THF (700 ml). Mixture was stirred for 30 min and then DIAD (39.3 ml, 0.20 mol) was added dropwise to the mixture. The reaction was stirred at 50 °C for 24 hours after which the mixture was evaporated to dryness and chromatographed on silica gel eluted with dichloromethane affording pure product (46.1 g) with 81% yield.

Elemental analysis for C₂₅H₄₀O (M ~ 372.6): calc. C 80.59, H 10.82, O 8.59%; found C 80.31, H 10.75%; ¹H NMR δH(CDCl₃): 9.86 (s, 1H), 7.80 (d, 2H, J ~ 8.8 Hz), 6.97 (d, 2H, J ~ 8.8 Hz), 5.34 (m, 2H), 4.03 (t, 2H, J ~ 6.4 Hz), 2.08 - 1.89 (m, 4H), 1.87 - 1.76 (m, 2H), 1.50-1.22 (m, 22H), 0.86 (t, 3H, J ~ 6.6 Hz); ¹³C NMR δC(CDCl₃): 189.97, 159.55, 131.64, 130.35, 130.24, 31.93, 29.80, 29.77, 29.66, 29.65, 29.64, 29.61, 29.56, 29.55, 29.48, 29.47, 29.39, 29.35, 29.34, 29.28, 29.25, 29.13, 28.21, 27.25, 26.06, 24.95, 22.71, 14.14

Synthesis of methyl 4-[(E)-2-{4-[(9Z)-octadec-9-en-1-yloxy]phenyl}ethenyl]benzoate (**2**)

Anhydrous potassium carbonate (12.26 g, 89 mmol) and 18-crown-6 (30 mg) were added to methyl 4-(triphenylphosphoniummethyl)benzoate bromide (**3**, 29.0 g, 58 mmol) suspended in dry dichloromethane (200 ml) and THF (250 mL) mixture and stirred at room temperature for about half an hour. 4-(octadec-9-enyloxy)benzaldehyde (**1**, 23.11 g, 0.048 mol) dissolved in tetrahydrofuran (100 ml) was added to the yellow reaction mixture and then the mixture was heated under reflux for 24 hours. After the inorganic salts were filtered off, the filtrate was evaporated to dryness and crystallized twice from ethanol affording **2** (10.7 g) with 44% yield.

Elemental analysis for C₃₄H₄₈O₃ (M ~ 504.7): calc. C(80.91%) H(9.59%) O(9.51%); found C 80.63, H 9.25%; ¹H NMR 200 MHz, δH(CDCl₃): 8.08 (d, 2H, J ~ 8.5 Hz), 7.58 (d, 2H, J₁~8.4 Hz), 7.49 (d, 2H, J ~ 8.5 Hz), 7.25 (d, 2H, J ~ 8.5 Hz), 6.91 (d, 2H, J ~ 8.6 Hz), 5.37 (m, 2H), 4.00 (t, 2H, J ~ 7.0 Hz), 3.90 (s, 3H), 2.04-1.95 (m, 4H), 1.88-1.73 (m, 2H), 1.50 - 1.24 (m, 22H), 0.88 (t, 3H, J ~ 6.8 Hz); ¹³C NMR δC(CDCl₃): 197.48, 159.55, 144.92, 143.12, 131.44, 130.66, 130.02, 127.54, 114.85, 31.93, 29.80, 29.77, 29.66, 29.65, 29.64, 29.61, 29.56, 29.55, 29.48, 29.47, 29.39, 29.35, 29.34, 29.28, 29.25, 29.13, 28.21, 27.25, 26.06, 24.95, 22.71, 14.14

Synthesis of 4-[(E)-2-{4-[(9Z)-octadec-9-en-1-yloxy]phenyl}ethenyl]benzoic acid chloride (**3**)

Methyl ester, **2**, (10.5 g, 20.8mmol) was dissolved in 600 mL of hot ethanol and 50 mL of THF and then potassium hydroxide (8.41 g, 0.15 mol) in hot ethanol (100 mL) was added. The reaction mixture was heated under reflux for 12 hours. White precipitate formed. After cooling down, crude salt was filtered, washed with copious amounts of ethanol and dried under vacuum. The white solid was suspended in toluene (50 mL) and excess of oxalyl chloride was added (10.5 mL). After filtration of the precipitated potassium chloride, the solvent was evaporated to dryness yielding yellowish product (9.53 g, 90%).

Synthesis of 4-hydroxyphenyl 4-[(E)-2-{4-[(9Z)-octadec-9-en-1-yloxy]phenyl}ethenyl]benzoate (**4**)

Triethylamine (1.8 mL) and DMAP (50 mg) was added to hydroquinone (14.3 g, 0.13 mol) solution in THF (250 mL) and stirred for 30 min at room temperature. Then 5.09 g (0.01 mol) of 4-[(E)-2-{4-[(9Z)-octadec-9-en-1-yloxy]phenyl}ethenyl]benzoic acid chloride (**3**) in 100 mL of THF was added and the reaction mixture was further stirred for 24 h at 55 °C. A precipitate of triethylamine hydrochloride formed which was filtered and the filtrate was evaporated to dryness. The crude product was crystallized three times from methanol and three times from toluene, affording **4** (4.70 g) with 62% yield.

Elemental analysis for C₃₉H₅₀O₄ (M ~ 582.8): calc. C 80.37, H 8.65, O 10.98%; found C 80.67, H 8.95%; ¹H NMR 200 MHz, δH(CDCl₃): 8.15 (d, 2H, J ~ 8.5 Hz), 7.60 (d, 2H, J₁~8.5 Hz), 7.48 (d, 2H, J ~ 8.5 Hz), 7.24 - 7.00 (m, 6H), 6.91 (d, 2H, J ~ 8.5 Hz), 5.36 (m, 2H), 3.99 (t, 2H, J ~ 7.0 Hz), 2.04-1.95 (m, 4H), 1.88-1.73 (m, 2H), 1.50 - 1.24 (m, 22H), 0.88 (t, 3H, J ~ 6.8 Hz); ¹³C NMR δC(CDCl₃): 164.91, 159.55, 152.18, 148.34, 143.12, 131.44, 130.66, 130.02, 127.54, 122.49, 117.53, 114.85, 31.93, 29.80, 29.77, 29.66, 29.65, 29.64, 29.61, 29.56, 29.55, 29.48, 29.47, 29.39, 29.35, 29.32, 29.28, 29.25, 29.12, 28.21, 27.26, 26.06, 24.95, 22.71, 14.15

Synthesis of 4-[(16-bromohexadecanoyl)oxy]phenyl 4-[(E)-2-{4-[(9Z)-octadec-9-en-1-yloxy]phenyl}ethenyl]benzoate (**5**)

DMAP (50 mg), 16-bromohexadecanoic acid (2.53 g, 7.56 mmol) and 4-hydroxyphenyl 4-[(E)-2-{4-[(9Z)-octadec-9-en-1-yloxy]phenyl}ethenyl]benzoate (**4**, 1.10 g, 1.89 mmol) were dissolved in tetrahydrofuran under argon atmosphere. Then N,N'-dicyclohexylcarbodiimide (DCC, 1.56 g, 7.56 mmol) in 20 mL of THF was added dropwise and the reaction was stirred for 24 h at 50 °C. A precipitate formed which was filtered and the filtrate was evaporated to dryness. It was then dissolved in chloroform (20 mL) and precipitated with methanol (20 mL), cooled to 4 °C, filtered, dried under vacuum and chromatographed on silica gel eluted with warm toluene, affording **5** (1.36 g) with 80% yield.

Elemental analysis for C₅₅H₇₉O₅Br (M ~ 900.1): calc. C 73.39, H 8.85, Br 8.88%; found C 73.11, H 8.55%; ¹H NMR 500 MHz, δH(CDCl₃): 8.15 (d, 2H, J ~ 8.5 Hz), 7.60 (d, 2H, J₁ ~ 8.5 Hz), 7.48 (d, 2H, J ~ 8.5 Hz), 7.24 - 7.00 (m, 6H), 6.91 (d, 2H, J ~ 8.5 Hz), 5.36 (m, 2H), 3.99 (t, 2H, J ~ 7.0 Hz), 3.41 (t, 2H, J ~ 7.0 Hz), 2.56 (t, 2H, J ~ 7.0 Hz), 2.04-1.95 (m, 4H), 1.88-1.73 (m, 6H), 1.50 - 1.24 (m, 44H), 0.88 (t, 3H, J ~ 6.8 Hz); ¹³C NMR δC(CDCl₃): 172.24, 164.91, 159.55, 148.34, 148.22, 143.12, 131.44, 130.66, 130.02, 129.83, 128.18, 127.54, 126.19, 125.10, 122.59, 122.49, 114.85, 68.14, 34.40, 34.08, 32.88, 31.93, 29.80, 29.77, 29.66, 29.65, 29.64, 29.61, 29.56, 29.55, 29.48, 29.47, 29.39, 29.35, 29.34, 29.28, 29.25, 29.13, 28.80, 28.21, 27.25, 27.22, 26.06, 24.95, 24.68, 22.71, 14.14

Synthesis of 4-[(16-sulfanylhexadecanoyl)oxy]phenyl 4-[(E)-2-[4-[(9Z)-octadec-9-en-1-yloxy]phenyl]ethenyl]benzoate (**6**), **L** in the main text

Bromide (5, 500 mg, 0.56 mmol) was dissolved under argon atmosphere in a dry and freshly degassed (1 h) THF (50 mL). Mixture was heated up to 40 °C and hexamethyldisilthiane (0.123 mL, 0.59 mmol, 1.05 eq.) was added quickly. After 5 minutes 0.56 mL (1M solution in THF) of tetra-*n*-butylammonium fluoride was added and solution turned greenish. The reaction mixture was stirred at 40 °C for 30 minutes, then it was allowed to reach room temperature and it was further stirred for 30 minutes. Then, 100 mL of dichloromethane was added and then mixture was washed three times with saturated NH₄Cl aqueous solution. Afterwards, the mixture was dried (MgSO₄) and the solvent was evaporated. The crude product was chromatographed on silica gel eluted with warm toluene (40 °C), affording **6** as a white solid (303 mg) with 64% yield.

Elemental analysis for C₅₅H₈₀O₅S (M ~ 721.4): calc. C 71.59, H 7.96; found C 71.32, H 7.99%; ¹H NMR 500 MHz, δH(CDC₃): 8.15 (d, 2H, J ~ 8.5 Hz), 7.60 (d, 2H, J₁ ~ 8.5 Hz), 7.48 (d, 2H, J ~ 8.5 Hz), 7.24 – 7.00 (m, 6H), 6.91 (d, 2H, J ~ 8.5 Hz), 5.36 (m, 2H), 3.99 (t, 2H, J ~ 7.0 Hz), 2.56 (t, 2H, J ~ 7.0 Hz), 2.52 (q, 2H, J ~ 7.0 Hz), 2.04-1.95 (m, 4H), 1.88-1.73 (m, 6H), 1.50 – 1.24 (m, 44H), 0.88 (t, 3H, J ~ 6.8 Hz); ¹³C NMR δC(CDC₃): 172.24, 164.91, 159.55, 148.34, 148.22, 143.12, 131.44, 130.66, 130.02, 129.83, 128.18, 127.54, 126.19, 125.10, 122.59, 122.49, 114.85, 68.14, 34.41, 34.08, 32.63, 31.93, 29.80, 29.77, 29.72, 29.66, 29.61, 29.55, 29.48, 29.39, 29.35, 29.34, 29.28, 29.25, 29.14, 29.11, 28.41, 27.25, 27.22, 26.06, 24.95, 24.68, 22.71, 14.14

2. Mesogenic ligand (**L**) phase sequence

Phase sequence for 4-[(16-sulfanylhexadecanoyl)oxy]phenyl 4-[(E)-2-[4-[(9Z)-octadec-9-en-1-yloxy]phenyl]ethenyl]benzoate (**L** in the main text); transition temperatures are given in °C and transition thermal effects (in parentheses) in Jg⁻¹:

Cry 83.1 (52.2) SmF 110.6 (5.9) SmC 148.3 (9.3) Iso

Liquid crystalline phases formed were identified based on the observation of characteristic optical textures under polarizing microscope, and the identification was confirmed by x-ray diffraction method – narrowing of the high angle signal related to in-plane intermolecular distances was observed in SmF phase. In both phases, SmC and SmF, the increase of smectic layer spacing was observed on cooling (Fig. S1), which can be attributed to stretching of molecules and growing orientational order of long molecular axes.

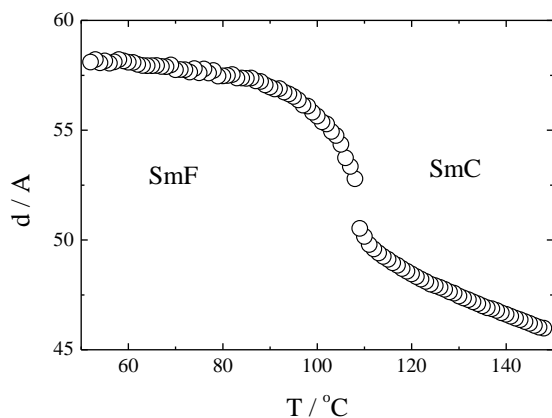


Figure S1 Layer spacing vs. temperature for the mesogenic ligand - 4-[(16-sulfanylhexadecanoyl)oxy]phenyl 4-[(E)-2-[4-[(9Z)-octadec-9-en-1-yloxy]phenyl]ethenyl]benzoate (**L** in the main text).

3. Gold nanoparticles synthesis (**G₈**)

Gold clusters using octanethiolas surface ligand was synthesized according to a modified Brust-Schiffrin protocol [S1], yielding **G₈** nanoparticles. An aqueous solution of hydrogen tetrachloroaurate (90 mL, 30 mmol dm⁻³) was extracted three times, each time with 200 mL of methyltriethylammonium chloride (5.57 g, 1.38 mmol) toluene solution to transfer all tetrachloroaurate ions to the organic layer. Toluene layer was separated and octanethiol was added to the organic solution (2 mol eq. in respect to AuCl₄⁻). The mixture was stirred for 15 min at room temperature. Then, freshly prepared aqueous solution of sodium borohydride (1.40 g, 30 mmol in 10 mL of cold H₂O) was quickly added under vigorous stirring. Immediately the solution turned dark brown and evolution of a gas was observed. After further stirring for 3 h the organic phase was separated, washed with deionized water (2x50 mL), concentrated to 5 mL using rotary evaporator and mixed with 200 mL of absolute ethanol to precipitate nanoparticles. The mixture was kept for 12 h at -4 °C. The dark

brown precipitate was sonicated for 60 s and centrifuged (5 min, 13 000 rpm). Supernatant was discarded, precipitate was dissolved in a small amount of toluene (5 mL) and again precipitated with ethanol (100 mL) and centrifuged. The procedure was repeated until no trace of excess of thiol was found, as determined by ^1H NMR spectra and TLC. Finally, all samples were dissolved in 20 mL of toluene and centrifuged (30 min, 13 000 rpm) to remove aggregates.

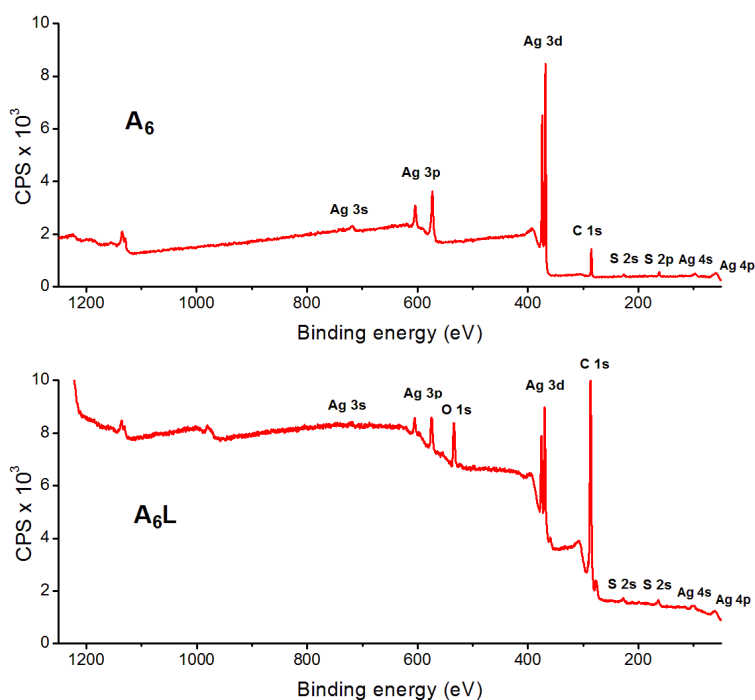
4. Silver nanoparticles synthesis (A_6)

Silver clusters using hexanethiol as surface ligand was synthesized according to a modified literature protocol [S2], yielding A_6 nanoparticles. 1.5 g dodecylamine was dissolved in 50 mL cyclohexane, then 12 mL aqueous formaldehyde (37%) was added. After vigorous stirring for 10 min at room temperature, the cyclohexane phase was separated out and washed twice with water (2 x 50 mL). Next, an aqueous solution of AgNO_3 (0.4 g AgNO_3 in 20 mL H_2O) was added to vigorously stirred cyclohexane solution. After few minutes the color of the organic phase turned dark brown. The mixture was left to stir for 40 min after which hexanethiol (1 molar eq. of dodecylamine) was added and the reaction was stirred overnight. Without this step the resulting nanoparticles covered with amine ligands agglomerated when centrifuged. Then, the aqueous phase was separated out and nanoparticles were precipitated by addition of 100 mL of ethanol. The dark brown precipitate was sonicated for 60 s and centrifuged (5 min, 6 000 rpm). The supernatant was discarded, the precipitate was dissolved in a small amount of cyclohexane (10 mL) and again precipitated with ethanol (100 mL) and centrifuged. The procedure was repeated until no trace of excess of thiol was found, as determined by ^1H NMR spectra and TLC. The resulting NPs were more stable than the nanoclusters with dodecylamine ligands obtained by the original procedure, which enabled usage of a precipitation/centrifugation protocol for the work up of the sample.

5. Hybrid nanoparticles synthesis

The A_6 and G_8 nanoparticles were used as starting material for the preparation of two hybrid nanoparticles, denoted as A_6L and G_8L . A ligand exchange reaction was performed following a procedure similar to that described elsewhere [S3]. To 20 mg of nanoparticles dissolved in 10 mL hexane/toluene mixture ($V/V=2/1$) 40 mg of **L** ligand was added. The reaction proceeded at 40 °C temperature for 24 h. No precipitation and/or change of color occurred. After 24 h the reaction mixture was concentrated to ca. 2 mL, nanoparticles were precipitated with 20 mL of acetone and centrifuged (13000 rpm, 5 min). Supernatant containing unbound thiol ligands was discarded. The precipitate was dissolved in 5 mL of warm toluene and precipitation/centrifugation process was repeated. This washing procedure was repeated until no traces of free mesogenic ligand remained, as determined by TLC. Then, all samples were redissolved in DCM (20 mL) and centrifuged (13000 rpm, 5 min) to remove any aggregates. The precipitate was removed and the solution was concentrated.

6. XPS analysis of A_6



30 **Figure S2** XPS survey analysis of A_6 (top image) and A_6L (bottom image) nanoparticles.

Table S1. Peaks positions and % atomic concentrations calculated based on XPS measurements of **A₆** and **A₆L** samples.

Nanoparticle type	Region name	Position	% Atomic Concentration
A₆	O 1s	-	0
	C 1s	285.0	53.04
	S 2p	162.0	8.59
	Ag 3d	368.2	38.37
A₆L	O 1s	532.6	6.72
	C 1s	285.0	85.76
	S 2p	162.2	2.41
	Ag 3d	368.2	5.11

5 Based on XPS measurements we were able to calculate the relative number of ligands attached to the surface of **A₆L** nanoparticles. First, we have calculated C/S atomic ratio for **A₆** NPs, which is c.a. $C/S_{A_6}=6$. Since **A₆** nanoparticles were covered with hexylthiol molecules (for which, based on the molecular formula C/S atomic ratio is 6) the number was as expected. Then, based on the % atomic concentrations we have calculated C/S atomic ratio for **A₆L** nanoparticles - $C/S_{A_6L}=35.58$. The relative atomic ratios C/S for hexylthiol (C/S=6) and ligand **L** (C/S=55) are known, therefore we used them to recalculate the C/S_{A_6L} atomic ratio to percentage of **L** population in **A₆L** nanoparticle organic corona: $\%L = (C/S_{A_6L}-6)/(55-6)$. It was estimated that c.a. 60% of the organic corona of **A₆L** sample was ligand **L**.

15 7. ¹H NMR analysis of **A₆L** and **G₈L**

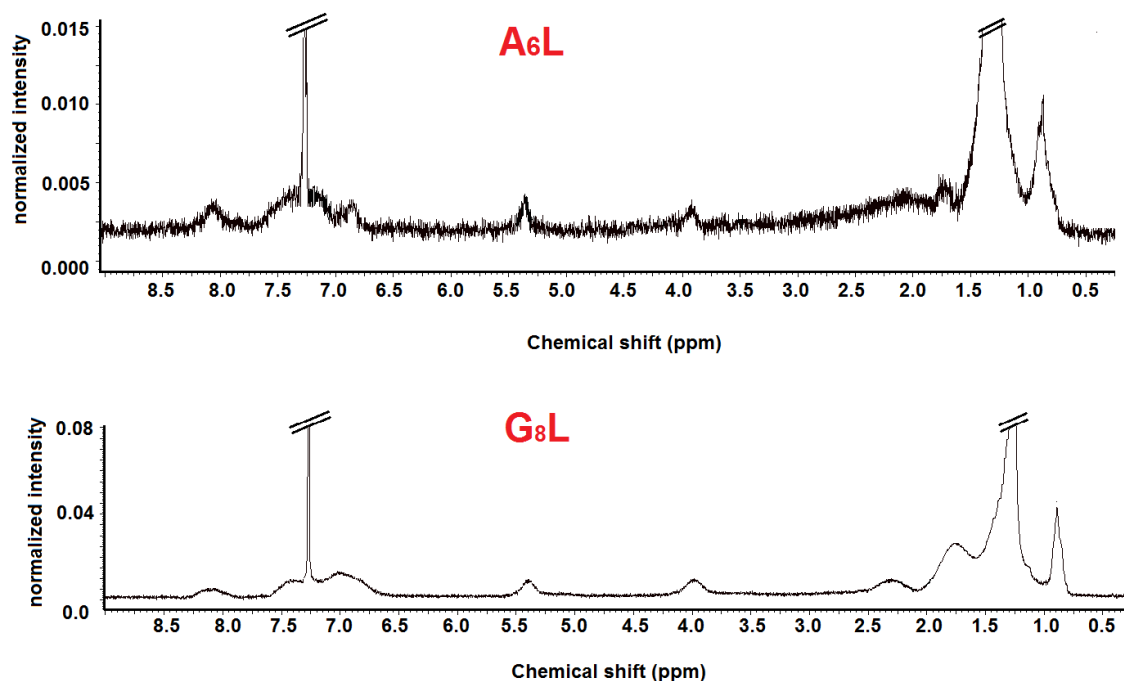


Figure S3 ¹H NMR analysis of **A₆L** and **G₈L** nanoparticles.

8. TGA analysis of **A₆**, **G₈**, **A₆L** and **G₈L**

To evaluate the exact composition of organic coronas of the studied nanoparticles, thermogravimetric analysis (TGA) was used. The weight losses for **A₆** and **G₈** (below 250 °C) were 14.7% and 19.6%, respectively. These values were attributed to the removal of the organic shell and were recalculated to the number of surface alkyl thiols (Table 1) as outlined below. TGA traces for hybrid nanoparticles revealed substantially larger weight losses in two distinct steps. The first one, below 250 °C can be attributed to the removal of alkyl thiol molecules and accounts for a mass drop of 4.2 and 6.5% for **A₆L** and **G₈L**, respectively. A wider peak at higher temperature values (>250 °C) is due to the removal of **L** molecules (weight losses 42.4 and 40.8% for **A₆L** and **G₈L**, respectively). The numbers of alkyl (N_{alkyl}) and mesogenic (N_{L}) molecules on the surface of a single NP are given in Table 1 in the manuscript.

First approach: To convert the mass loss measured by the TGA measurements to surface ligand stoichiometry we first calculated the mass of single metal spheres for silver (M_{Ag}) and gold (M_{Au}) nanoparticles, using the diameter derived from SAXS and TEM and the bulk density of metals $\rho_{\text{Ag}} = 10.49 \text{ [g/cm}^3\text{]}$, $\rho_{\text{Au}} = 19.3 \text{ [g/cm}^3\text{]}$. The calculated masses were: $M_{\text{Ag}} = 4.7 \times 10^{-19} \text{ g}$ and $M_{\text{Au}} = 1.4 \times 10^{-19} \text{ g}$. The mass of organic matter (M_{org}) removed from a single nanoparticle was calculated using % of mass left after the analysis ($\%M_{\text{left}}$) and % of mass loss ($\%M_{\text{loss}}$): $M_{\text{org}} = M_{\text{Ag(or Au)}} / (\%M_{\text{left}} * \%M_{\text{loss}})$. $\%M_{\text{left}}$ and $\%M_{\text{loss}}$ can be read out of Fig. S2. To retrieve the number of ligands per nanoparticle M_{org} has to be divided by the mass (in [g]) of the ligand responsible for the given mass drop: $m_{\text{C}_6\text{H}_{13}\text{SH}} = 1.95 \times 10^{-22} \text{ g}$, $m_{\text{C}_8\text{H}_{17}\text{SH}} = 2.43 \times 10^{-22} \text{ g}$, $m_{\text{L}} = 1.42 \times 10^{-21} \text{ g}$. For nanoparticles after the exchange reaction mass losses below and above 250°C were treated separately. Numbers of ligands per nanoparticle are given in Table 1 in the main text. Correctness of the calculations was confirmed with organic matter density estimation for **A₆L** and **G₈L** nanoparticles, yielding 1.0 and 0.9 g/cm³, respectively.

Second approach: Another way of interpreting TGA traces for **A₆L** and **G₈L** samples is to use the total mass drop to calculate the surface ligand stoichiometry. The mass of the organic matter removed from a single nanoparticle can be calculated as presented above. Though, to calculate the surface ligand stoichiometry an assumption has to be made that the number of ligands in **A₆L** and **G₈L** samples is the same as in the **A₆** (414) and **G₈** (140) nanoparticles, respectively. With this assumption an average molar mass of the removed ligands can be calculated - $M_{\text{average}} = M_{\text{org}} / N_{\text{alkyl}} * N_{\text{A}}$, where N_{A} is the Avogadro number. Then, based on the molar masses of alkyl (M_{alkyl}) and **L** (M_{L}) ligands the population of **L** ligands can be calculated as follows: $\%L = (M_{\text{average}} - M_{\text{alkyl}}) / (M_{\text{L}} - M_{\text{alkyl}}) * 100\%$.

The population of **L** ligands in the organic shells of **A₆L** and **G₈L** samples based on the first approach (with the discriminating between mass losses below and above 250°C) presented above yields 58 and 52%, respectively. With the second approach (the total mass loss and assumption as for the total number of ligands) the numbers are 65 and 55%, respectively. Both approaches yield population of **L** ligands in the gold nanoparticles which are in very good agreement. On the other hand, the difference in the population of **L** ligands in the silver nanoparticles is based on those two approaches 7%. XPS measurements support show that 60% of the ligands are the mesogenic ones (**L**), closer to 58% from the first TGA calculation strategy. Together with distinct peaks observed in the derivative of TGA traces, confirming clear discrimination between mass drops below and above 250°C (Fig. S4), it can be concluded that the first approach is the right one.

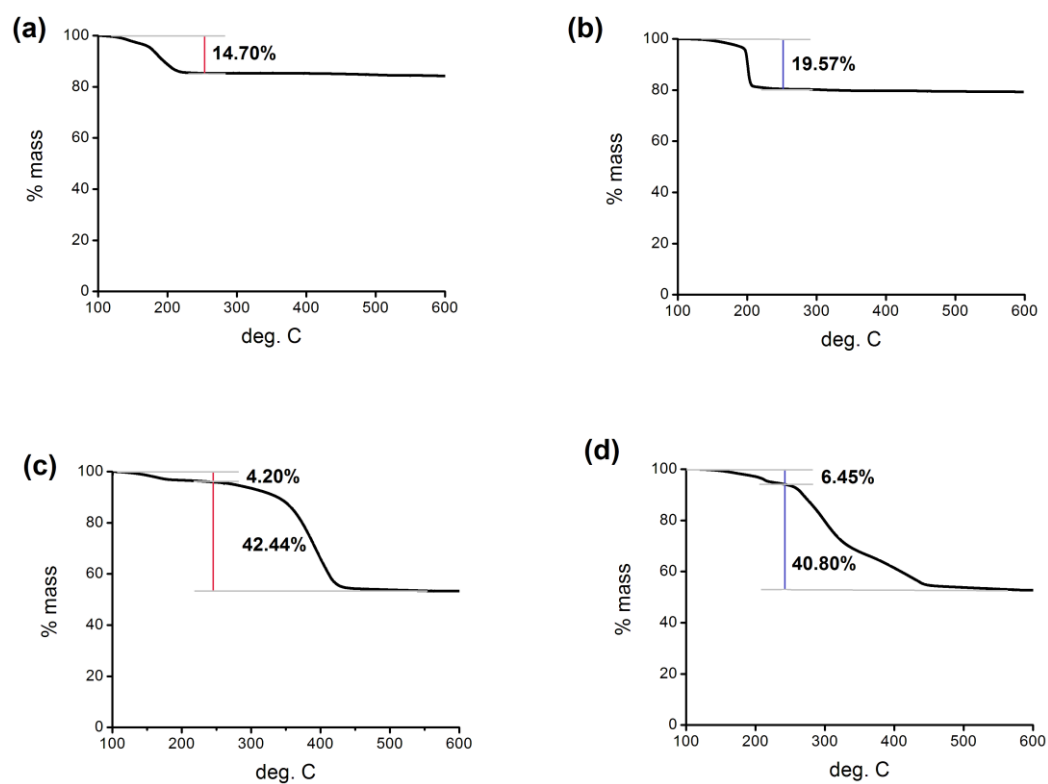


Figure S4 TGA analysis of (a) A_6 , (b) G_8 , (c) A_6L and (d) G_8L nanoparticles; % of mass drops below and above 250 °C are given in pictures.

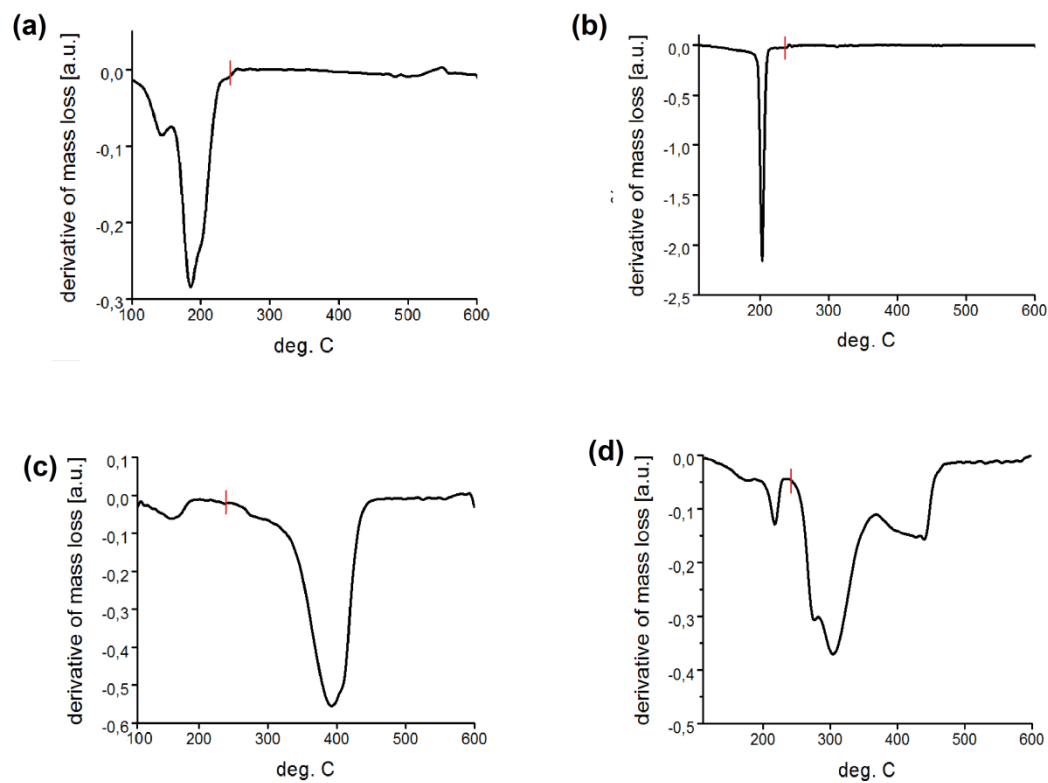


Figure S5 Derivative of TGA traces (a) A_6 , (b) G_8 , (c) A_6L and (d) G_8L nanoparticles shown in Figure S4; red line points 250°C.

9. SAXS and SAXRD analysis of A_6 , G_8 , A_6L and G_8L

The introduction of the liquid-crystalline ligand onto the surface of nanoparticles resulted in a change of interparticle distances as measured by small-angle X-ray diffraction (SAXRD). For G_8 a broad peak was observed at ~ 3.4 nm, whereas for G_8L a strong signal is observed at ~ 7.5 nm and a weaker one at ~ 3.6 nm. For both G_8 and G_8L materials no long-range ordering is observed. The diffraction pattern of A_6 exhibits a signal at ~ 5.2 nm, while for A_6L the reflections correspond to ~ 9.1 and ~ 5.7 nm (the latter being substantially weaker). The X-ray results are consistent with TEM studies, the images taken for A_6L sample show some degree of 2D local ordering of nanoparticles (Figure 2 in the main text), with two distinct interparticle distances, corresponding well to those derived from SAXRD. Thus, we conclude that for both G_8L and A_6L ligand exchange increases the interparticle distances but also causes short, chain-like structures to appear, indicating that some anisotropy of the organic shell occurs.

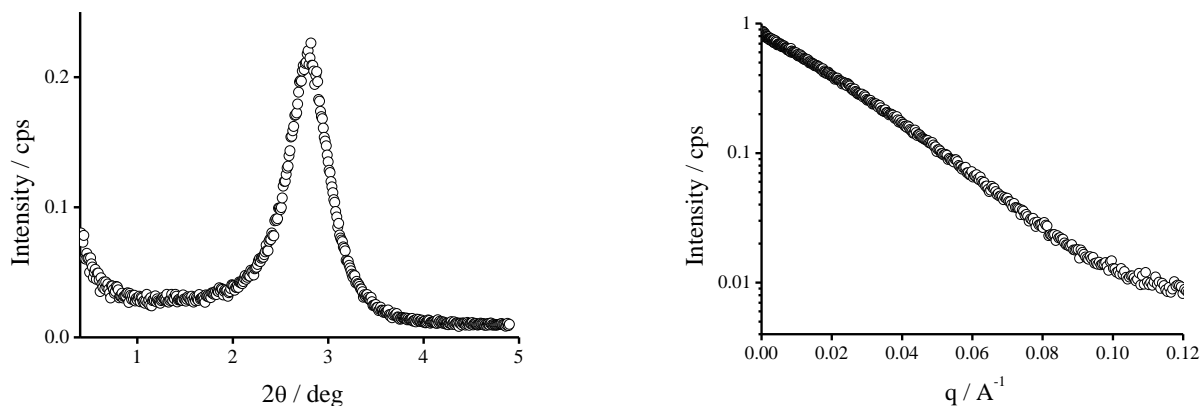


Figure S6 (left) Diffraction pattern obtained for G_8 nanoparticles in a condensed state - dropcasted on the kapton foil. The peak position corresponds to the mean nanoparticle diameter, including organic coating - 3.2 nm. (right) Guinier plot for G_8 particles dissolved in toluene; assuming non-interacting spherical particles of mean radius was calculated as 1.2 nm and standard deviation 0.16 nm.

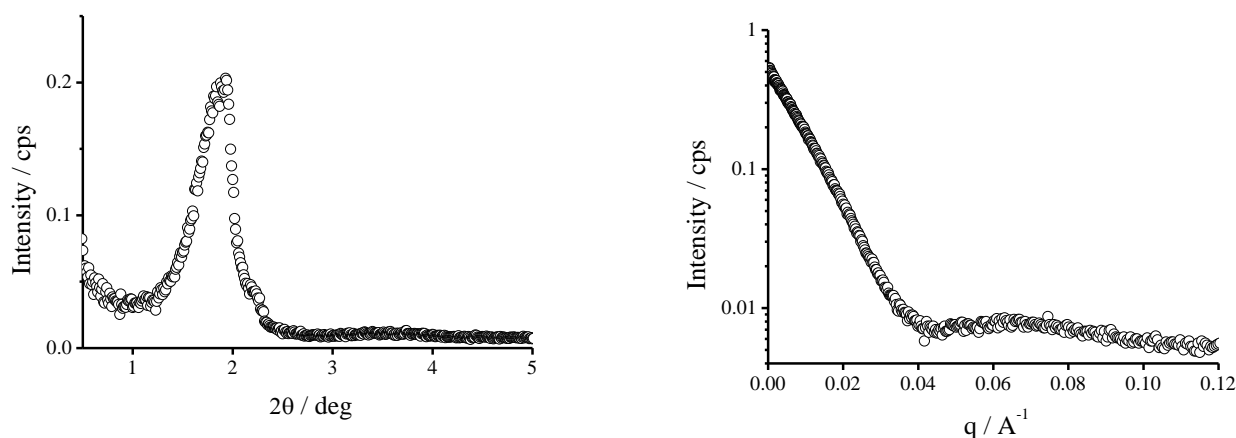


Figure S7 (left) Diffraction pattern obtained for A_6 nanoparticles in a condensed state - dropcasted on the kapton foil. The peak position corresponds to the mean nanoparticle diameter, including organic coating - 3.2 nm. (right) Guinier plot for A_6 particles dissolved in toluene; assuming non-interacting spherical particles of mean radius was calculated as 1.2 nm and standard deviation 0.16 nm.

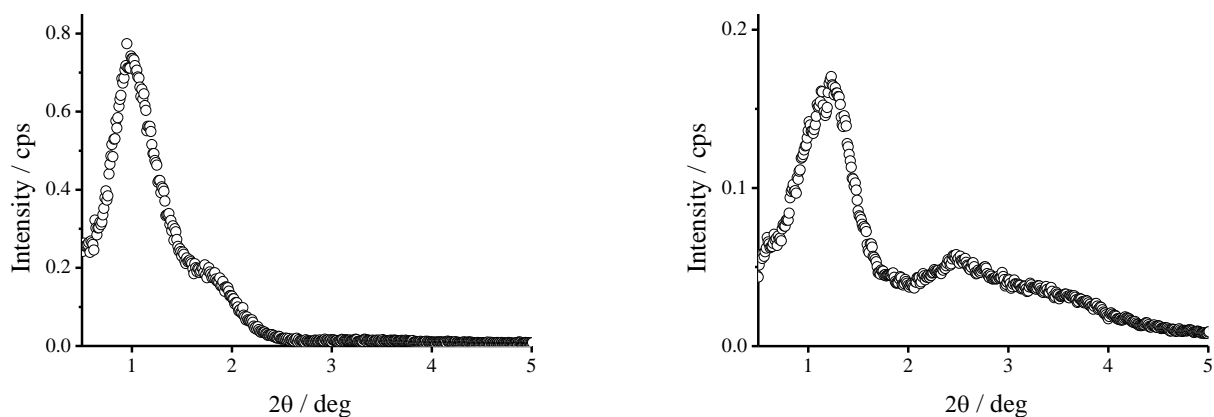


Figure S8 (left) Diffraction pattern obtained for **A₆L** nanoparticles in a condensed state - dropcasted on the kapton foil. The peak position corresponds to the mean nanoparticle diameter, including organic coating - 9.1 nm; a weaker signal at 5.7 nm is due to local ordering of the nanoparticles; (right) Diffraction pattern obtained for **G₈L** nanoparticles in a condensed state - dropcasted on the kapton foil. The peak position corresponds to the mean nanoparticle diameter, including organic coating - 7.5 nm; a weaker signal at 3.6 nm is due to local ordering of the nanoparticles.

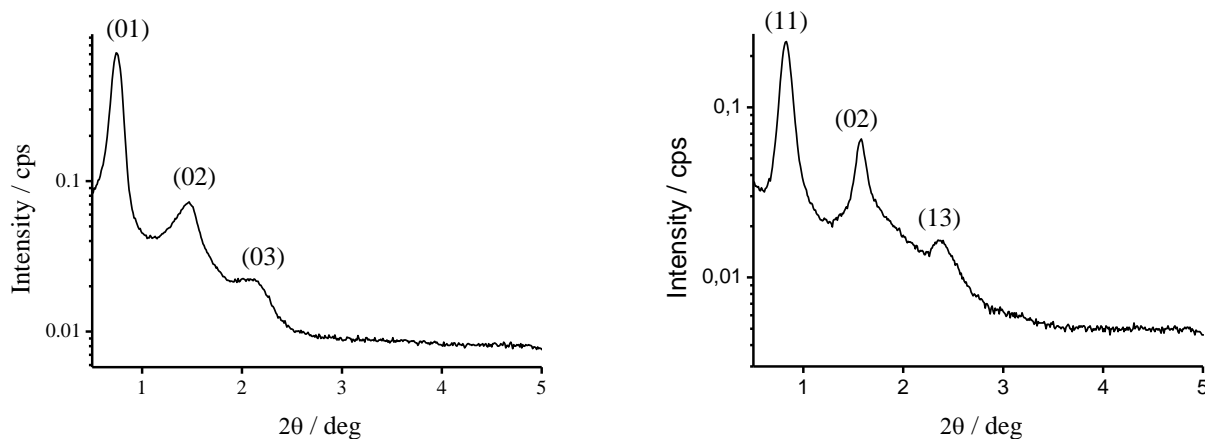


Figure S9 Integrated SAXRD profiles from Figure 3 in the main text, peaks indexation is given; (left) **A₆L**, (right) **G₈L**.

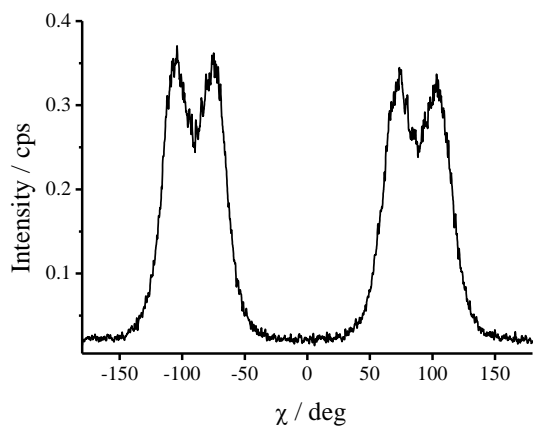


Figure S10 Signal intensity changes along a circle of radius corresponding to (11) signal position in **G₈L** diffractogram shown in Figure 3 in the main text, evidencing azimuthal signal splitting typical for modulated smectics.

10. TEM analysis of gold nanoparticles

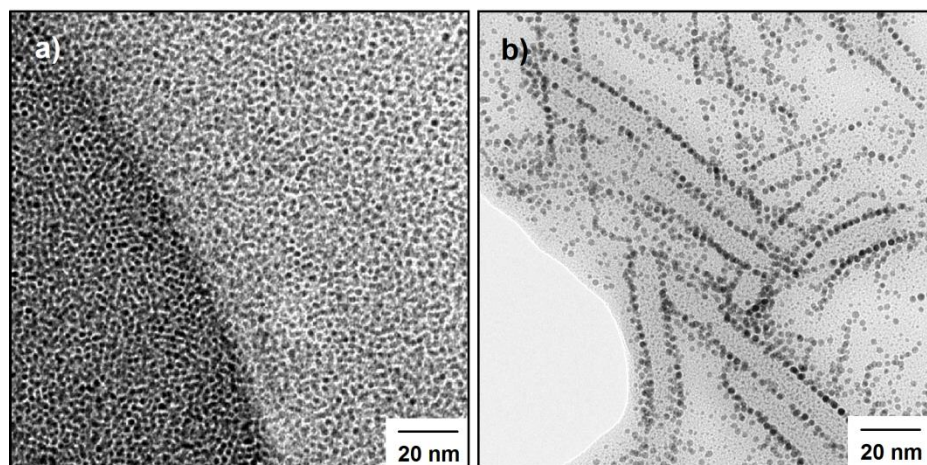


Figure S11 TEM images of gold nanoparticles: (a) G_8 as dropcasted, (b) G_8L thermally annealed; G_8 NPs exhibit isotropic packing with mean interparticle distance ~ 3.5 nm, while G_8L NPs show packing with two characteristic distances, interlayer ~ 11.6 and in-plane ~ 4.3 nm, evidencing the tendency to form lamellar structures; the inlayer and interlayer distance values correspond well to those obtained from XRD studies.

11. Polarized Optical Microscopy analysis of A_6L

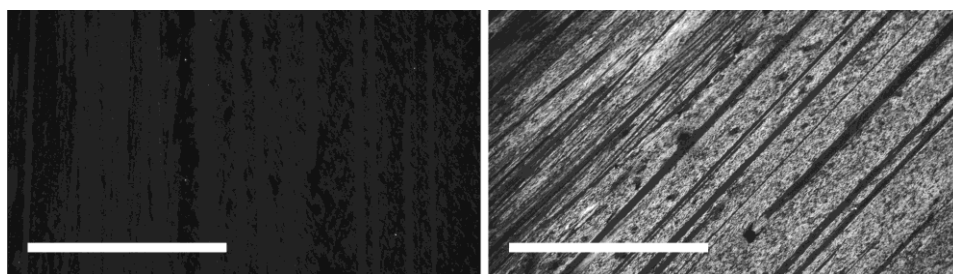


Figure S12 Polarized optical microscopy images of an annealed, oriented A_6L sample. The director is parallel with (left) and at 45° from (right) the horizontal. The crossed analyzer and polarizer were parallel to the sides of the images. The bar represents 0.5 mm. Identical lighting and exposure conditions were used, on the same sample spot.

12. Polarized IR studies

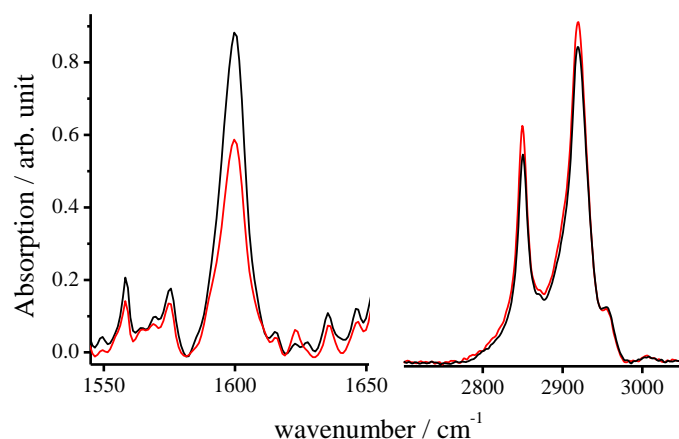
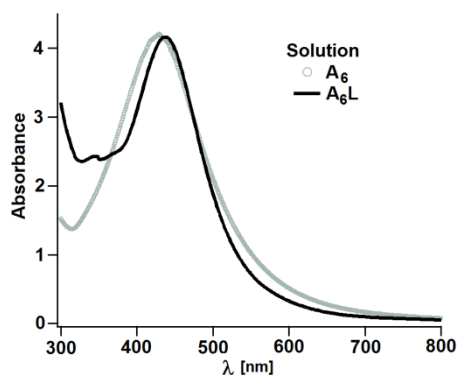


Figure S13 Chosen bands of the polarized IR absorption spectra for A_6L hybrid sample aligned by shearing. Signal at 1600 cm^{-1} is due to stretching of phenyl rings and those at 2850 cm^{-1} and 2920 cm^{-1} are due to CH_2 groups stretching. Black curve corresponds to the polarization of the incident IR beam along the shearing direction, while the red one to a perpendicular orientation.

13. UV-Vis measurements of A₆ and A₆L nanoparticles solutions



5 **Figure S14** UV-Vis absorption spectra of A₆ (in cyclohexane) and A₆L (in dichloromethane).

14. Surface plasmon resonance shift calculations

The UV-Vis absorption spectrum of noble metal particles exhibits a peak associated with their plasmon resonance. The position of the peak maximum λ_{max} is very sensitive to the particle environment, such as the dielectric constant of the host medium.

For A₆L particles in dilute solution plasmon absorption is observed at $\lambda_{\text{max}} \sim 440$ nm. For the drop-casted sample, the peak shifts to ~ 515 nm and becomes broader, signaling an increase in the effective refractive index n of the medium resulting from the change of host (n changes from 1.42 for dichloromethane to about 1.6 for a typical mesogen) and high volume fraction of particles (ϕ , of the order of 0.1). The particle size is much smaller than the wavelength, therefore their effect on the refractive index can be accounted for via an effective medium approach, such as the Maxwell-Garnett formula [S4]. The variation of λ_{max} due to a change in n is described by the formula $\lambda = \lambda_p \times (\epsilon^0 + 2\epsilon_m)^{1/2}$ [S5], where λ_p is the metal's bulk plasma wavelength calculated based on the literature value of silver bulk plasma frequency: 1.38×10^{16} . The high frequency dielectric constant (ϵ^0) was set to 5, as estimated by others [S5]. Birefringence, Δn , for the oriented anisotropic A₆L sample was estimated based on $\Delta\lambda_{\text{max}}$ shift when polarization of the incident light is changed from the direction along to the direction perpendicular to the layer normal. The ordinary refractive index of the sample was assumed to be 1.6 (typical for liquid crystals) and the extraordinary refractive index was changed to fit the experimentally observed λ_{max} shift.

REFERENCES

- 25 [S1] M. Brust, M. Walker, D. Bethell, D. J. Schiffrin and R. Whyman *J. Chem. Soc., Chem. Commun.*, 1994, **801**.
[S2] Chen, Y.; Wang, X. *Mater. Lett.*, 2008, **62**, 2215.
[S3] R. S. Ingram, M. J. Hostetler and R. W. Murray, *J. Am. Chem. Soc.* 1997, **119**, 9175.
[S4] W. T. Doyle, *Phys. Rev. B*, 1989, **39**, 9852.
[S5] P. Mulvaney, *Langmuir*, 1996, **12**, 788.

30